



CHORUS

This is the accepted manuscript made available via CHORUS. The article has been published as:

Thermal properties of nanoporous gold

Anatoly I. Frenkel, Relja Vasić, Bluma Dukesz, Diya Li, Mingwei Chen, Ling Zhang, and
Takeshi Fujita

Phys. Rev. B **85**, 195419 — Published 10 May 2012

DOI: [10.1103/PhysRevB.85.195419](https://doi.org/10.1103/PhysRevB.85.195419)

Thermal properties of nanoporous gold

Anatoly I. Frenkel,^{1*} Relja Vasić,¹ Bluma Dukesz,¹ Diya Li,² Mingwei Chen,³

Ling Zhang,³ Takeshi Fujita^{3,4}

¹*Department of Physics, Yeshiva University, 245 Lexington Avenue, New York, New York
10016, USA*

²*Department of Chemical and Biomolecular Engineering, University of Pennsylvania,
Philadelphia, Pennsylvania 19104, USA*

³*WPI Advanced Institute for Materials Research, Tohoku University, Sendai 980-8577,
Japan*

⁴*JST, PRESTO, 4-1-8 Honcho Kawaguchi, Saitama 332-0012, Japan*

Abstract

We measured the thermal expansion coefficient and Debye temperature of nanoporous gold (NPG) using Extended X-ray Absorption Fine Structure technique. Reduction of the nearest neighbor distances in NPG by ca. 0.01 Å compared to the bulk gold was attributed to the surface tension caused, in turn, by the finite size effect of the NPG ligaments. We also obtained that the Debye temperature in NPG is 5% lower than in bulk gold. We interpreted these observations in the framework of a bimodal distribution of surface and bulk bonds with different values of Debye temperature. The surface bonds with low Debye temperature extend within ca. 4 layers of Au atoms located on the pore surface, in a good agreement with prior resistivity measurements and theoretical predictions.

PACS number(s): 63.22.Dc, 61.05.cj, 65.40.De, 63.22.-m

*Corresponding author: Anatoly.Frenkel@yu.edu

I. Introduction

Nanoporous gold (NPG) received much attention during the last decade as an unsupported catalytic system¹⁻³ and as an attractive material in the field of sensors,⁴ actuators and optics.⁵ Their enhanced catalytic properties for CO oxidation are often attributed, much like in nanoparticle catalysts, to the presence of undercoordinated Au atoms.⁶⁻⁸ Among other factors that have been recently discussed in terms of their potential influence on the catalytic activity of NPG are: surface to volume ratio, mechanical strain, as well as the role of residual Ag.⁵

Among these factors, the strain effect on reactivity in nanoscale metal catalysts is a topic of intense experimental and theoretical research. As previously shown, the surface strain-induced change in the metal-metal distances affects adsorbate binding energy.^{9, 10} Strasser, et al¹⁰ interpreted the surface strain effect on reactivity in the framework of the d-band center model,¹¹ by noting that the compressive or tensile strain causes shift in d-band relative to the Fermi energy and that, in turn, changes the ligand binding energy. Similar to the static (configurational) disorder of atomic bonds at the surface of nanocatalysts, their nonbulklike dynamic (vibrational) disorder is also predicted to strongly influence on their reactivity.¹²

Analogously to metal nanoparticles, structural dynamics of nanoporous gold is expected to be modified by the nonbulklike structural and thermal properties of atoms residing in the pore surface. Despite the interest to such finite size effects in nanomaterials in general, and in the NPG in particular, no reports exist, to the best of our knowledge, on thermal expansion or Debye temperature measurements of the NPG, despite very intriguing theoretical prediction of its anomalously low value.¹³ Such investigations are particularly challenging due to the need to probe both the structure and dynamics of the surface atoms as a function of temperature and pressure, and to do so by maintaining high spatial and temporal resolution in order to sense both static and dynamic bond length characteristics. In this work we applied the by Extended X-ray Absorption Fine-Structure (EXAFS) method that was successfully used to analyze structural and thermodynamic properties of many bulk¹⁴⁻¹⁶ and nanoscale^{17, 18} systems. EXAFS is a premier technique for investigations of nanomaterials due to its excellent

spatial resolution (the bond lengths can be obtained with an accuracy of 0.005 Å or better) and its sensitivity to atomic vibrations, including anharmonic contributions.^{19, 20}

In the next Section we present experimental details on synthesis, scanning electron microscopy characterization and EXAFS measurements of NPG. Section III describes the data processing and analysis. Results are presented in Section IV and their discussion is given in Section V. Conclusions are presented in Section VI.

II. Experimental details

NPG is prepared by dealloying of Au alloy with other component, most commonly, Ag.^{21, 22} The precursor Ag₆₅Au₃₅ (atomic ratio) leaves with dimensions of 20 mm × 20 mm × 700 nm were annealed at 573 K for 3 hours to eliminate strain effect. Free-standing NPG sheets were then fabricated by chemically de-alloying precursor thin films in a 69% HNO₃ solution for 1 h at room temperature. The dealloyed samples were rinsed by deionized water (18.2 M Ω·cm) for more than three times to remove the residual chemical substances within the nanopore channels.

The morphology and structure of the NPG were investigated using a field-emission scanning electron microscope (JEOL JIB-4600F, 15 keV). A cyclic voltammograms of NPG membrane in 0.1 M HClO₄ solutions was obtained with an electrochemical workstation (Ivium Technology). The surface area was estimated using the reduction peak of the Au oxide. The characteristic ligament length scale was measured using Fast Fourier Transform (FFT) method.²³

EXAFS data were acquired at beamlines X19A and X18B of the NSLS at Brookhaven National Laboratory in transmission mode using the Au L₃ edge. The samples were prepared by stacking several NPG foils to provide sufficient absorbance (that corresponded to the edge jump of ca. 0.6) at the Au L₃ edge. The sample was loaded into the dedicated cell for EXAFS studies²⁴ that can be carried out within a temperature range from ca. 130 K to ca. 800 K. A bulk Au foil was measured simultaneously with the NPG sample (in reference mode) for energy alignment and calibration purposes. Multiple scans (up to 4) were collected at each temperature of interest and averaged in order to improve the signal-to-noise ratio. Measurements were done at different temperatures

under H₂ (5 % H₂ balanced with He for a total flow rate of 50 ml/min) atmospheres. Bulk Au and Ag samples were also measured in the same conditions and similar temperatures as the NPG samples. The lowest temperatures were 133 K (bulk Au), 163 K (NPG), and 183 K (bulk Ag). The rest of the temperatures were the same for all samples studied: 298, 393, 488, 583 and 673 K. As the structure of NPG is reported to coarsen when annealed at temperatures above 423-473 K,⁴ the last 2 temperature points were used for evaluating coarsening effects on EXAFS data.

III. Data processing and analysis

In EXAFS technique, the information about structural environment, including its dynamic changes, of the x-ray absorbing atom and its surroundings is extracted from the x-ray absorption coefficient $\mu(E)$ measured within 1000-1500 eV from the x-ray absorption edge energy. The oscillatory part of $\mu(E)$ results from the interference patterns of photoelectrons due to their scattering from neighboring atoms. It thus contains quantitative information about the local atomic environment in the proximity of the absorbing atom. The EXAFS signal $\chi(k)$ that originates from the nearest group of neighbors at approximately equal distances from the absorbing atoms (i.e., within the 1st shell), is often written as:²⁵

$$\chi(k) = \frac{S_0^2 N}{kR^2} |f^{\text{eff}}(k)| \sin \left[2kR - \frac{4}{3} \sigma^{(3)} k^3 + \delta(k) \right] e^{-2\sigma^2 k^3} e^{-2R/\lambda(k)}, \quad (1)$$

where k is the photoelectron wave number, $f^{\text{eff}}(k)$ and $\delta(k)$ are the photoelectron scattering-path amplitude and phase, respectively, S_0^2 is the passive electron reduction factor, N is the degeneracy of the scattering path (equal to the coordination number for the single-scattering paths), R is the effective half-path-length (which equals the interatomic distance for single-scattering paths), σ^2 is the mean-square deviation in R , also known as the second cumulant of the pair distribution function,²⁶ $\sigma^{(3)}$ is the third cumulant and $\lambda(k)$ is the photoelectron mean free path.

In order to extract thermal and structural parameters of NPG from EXAFS data we applied correlated Einstein model²⁷ that proved effective in many previous studies of

bulk^{28, 29} and nanoscale³⁰⁻³³ metals. In this model, parameters k_0 and k_3 of the anharmonic potential, $V(x) = (1/2)k_0x^2 + k_3x^3$, where $x = r - r_0$ is the deviation of the bond length r from the location of the potential minimum, can be obtained from the temperature dependence of the second and third cumulants of the effective pair distribution function.²⁷ The same two cumulants can be used to approximate the thermal expansion coefficient, α . In the limit of high temperature (where the quantum effects are negligible), Frenkel and Rehr obtained:²⁷

$$\sigma_d^2 \cong \frac{k_B T}{k}; \quad \sigma^{(3)} \cong -\frac{6k_3}{k^3}(k_B T)^2; \quad \alpha \cong -\frac{3k_3 k_B}{k^2 r}, \quad (2)$$

where σ_d^2 is the mean-square vibrational (dynamic) bond length disorder, T the absolute temperature, $k = k_0 + 6k_3\langle y \rangle$ the effective spring constant, y is the deviation from the equilibrium value of x at temperature T , and the brackets denote a thermal average.

Data processing and analysis with performed with IFEFFIT package.³⁴ The useful data ranges in k-space varied from 2 to 18.5 \AA^{-1} at the lowest temperatures to 2-10.5 \AA^{-1} at the highest temperatures. Data fitting was performed by calculating theoretically the photoelectron scattering functions for the first shell Au-Au contribution in bulk Au using FEFF6 program.²⁵ They were combined into EXAFS equation (1) which contains electronic (S_0^2 , and the photoelectron energy origin correction, ΔE_0) and structural parameters (e.g., N , R , σ^2 and $\sigma^{(3)}$). These parameters were adjusted for all temperature data concurrently, by applying multiple constraints in the analysis. The disorder parameters at all temperatures were constrained to follow the correlated Einstein model²⁷ which allowed to separately evaluate the temperature-independent, static disorder, and the temperature-dependent, dynamic disorder:²⁴ $\sigma^2(T) = \sigma_s^2 + \sigma_d^2(T)$. The last term in the right hand side is simply related to the Einstein temperature Θ_E via the effective spring constant in Eq. (2): $k = \mu\omega^2$, where μ is the reduced mass of the atomic pair and $\omega = k_B\Theta_E/\hbar$ is the effective bond vibration frequency (the mean of the projected density of modes).²⁷ Using the approximate relationship:³⁵ $\Theta_D \approx 1.27\Theta_E$ between the Debye and

Einstein temperatures, we also estimated Debye temperatures of Au, Ag and NPG after the best fit values of Einstein temperatures were obtained.

In the fits to the bulk metals (Au and Ag), the coordination numbers of the first nearest neighbor (1NN) bonds were fixed at 12 as expected in the face center cubic lattice. The best fit values of S_0^2 were found to be 0.873(14) and 0.947(19), respectively. In order to break the correlation between the amplitude factors in the fit, the S_0^2 parameter of the NPG was fixed to that of bulk Au (0.873). The following parameters were varied in the EXAFS analysis: the corrections to the photoelectron energy origin (the same at all temperatures), the Au-Au coordination number (the same at all temperatures), the nearest neighbor bond lengths (6 variables), the third cumulant of the 1NN pair distribution function (6 variables), and the values of Θ_E and σ_s^2 . The total number of relevant independent data points was 74, i.e., much greater than the total number of variables (16).

IV. Results

A SEM micrograph of the as-prepared NPG is shown in Fig. 1. The average gold ligament size is ca. 21 nm in length, with the minimum ligament width of 5 nm. The surface-to-volume ratio $\eta = A/V$ was measured to be $(9.2 \pm 0.9) \times 10^7 \text{ m}^{-1}$.

Representative raw EXAFS data in k -space and r -space are shown in Fig. 2. It is evident that the local structure in NPG is different from that in Au foil, and the difference is particularly noticeable in the 1NN peak region. The reduction in intensity of the NPG can be caused by either the reduced coordination number compared to the bulk, the increased bond length disorder or both. Although it is possible to separately evaluate these two effects in nanoparticles, where the coordination numbers are much smaller than in their bulk counterparts,³⁶⁻³⁸ in the case of the NPG the discrimination between these two contributions at the single temperature is complicated. Obtaining this information from EXAFS is much easier by utilizing strong temperature dependence of EXAFS amplitude and phase (Fig. 2 b). In the case of the NPG where the coordination number of the Au-Au pairs is expected to be close to 12 (and it was obtained to be nearly 12.0, within the ± 0.3 experimental uncertainty), we fixed the coordination number to be the

same at all temperatures, and separately obtained the best fit results for the coordination number and the values of $\sigma^2(T)$. Additional details are evident in Fig 2 b): as the temperature increases, the mean 1NN peak position shifts to lower r values. It would've been unphysical for bulk metals with closed packed structure to show negative thermal expansion (NTE),³⁹ but in this case the explanation is not the NTE but the anharmonicity of the Au-Au pair potential. Indeed, as was obtained before for bulk Pt, the anharmonic correction to the pair potential increases with temperature and, hence, the phase of EXAFS oscillation may decrease (and thus the peaks shift to the left) despite the increase in the 1NN bond length with temperature.³⁰ Representative data and fits are shown in Fig. 3 for two different temperatures. The best fit results for the Au-Au distances are shown in Fig. 4. The second and the third cumulants of the pair distribution function are shown in Figs. 5a and b, respectively, together with the linear fits with Eqs. (1). Table 1 contains the best fit values of the Einstein and Debye temperatures of bulk Au, Ag and the NPG, as well as their thermal expansion coefficients, effective force constants k and the anharmonic parameter k_3 obtained from the fits of Eq. (3) to the experimental data on the second and third cumulants.

V. Discussion

The Au-Au distances in the NPG decrease significantly compared to the bulk Au at temperatures less than 500 K, i.e., below the temperature when the NPG starts coarsening (Fig. 4). Such reduction cannot be explained by residual Ag present in our NPG sample after dealloying. Indeed, Au-Ag alloy shows very little change in Au-Au distance with concentration of Ag.⁴⁰ In the NPG, we estimated (by relative Au and Ag edge steps analysis) the concentration of residual amount of Ag as 6%. Ag K-edge EXAFS data indicates that it is predominantly alloyed with Au. For such a small concentration of Ag, temperature dependence of Au-Au bond of the bulk Au-Ag alloy was shown to be virtually the same as in bulk Au,⁴⁰ contrary to what we observed in the NPG (Fig. 4). Therefore, we conclude that the large reduction in Au-Au distance in the NPG compared to the bulk is likely the result of finite size effects rather than alloying with Ag. Kluth et al, reported that 0.01 Å bond length contraction (relative to the bulk) in Au nanocrystals as large as 8.5 nm in size,⁴¹ i.e., comparable to the size of ligaments of our NPG where

the minimum width was obtained to be 5 nm. Our results suggest that the bond length contraction in NPG has the same origin (surface tension) as in other low dimensional, unsupported Au systems.⁴²

Debye temperatures for bulk Au and Ag obtained in our analysis (Table 1) are in good agreement with other measurements (e.g., 175 K⁴³ and 184.6 K⁴⁴ for Au and 225 K⁴³ for Ag). Thermal expansion coefficients obtained for bulk Au and Ag (Table 1) agree well with their reported values: $1.4(1) \times 10^{-5} \text{ K}^{-1}$,⁴⁵ and $1.5 \times 10^{-5} \text{ K}^{-1}$,⁴⁶ respectively. We conclude, by noting a good agreement between our EXAFS results and those from literature for thermodynamic properties of bulk Au and Ag, that our procedure is well calibrated on standard compounds and can be applied to investigate the unknown, i.e., the NPG. The intriguing new results obtained for the NPG are the reduction of the Einstein and, hence, Debye temperatures (Table 1).

The nanoscale size effect on Debye temperature is far from being understood. Although it is well established that the surface atoms and inner atoms have different vibration frequencies (and thus the surface layer and the interior of the crystal should have different Debye temperatures),⁴⁷ the magnitude, and even the sign, of the effect depend very strongly on a particular system. For example, reduction of Debye temperature to 160 K have been previously observed in the smallest Au nanoparticles supported on amorphous silica in the 2.4 to 5nm range and attributed to the finite size effect causing the surface atoms to have smaller vibrational frequency compared to the bulk.⁴⁸ In Pt nanoparticles supported on γ -alumina, the opposite effect was observed: their Debye temperature was greater than in the bulk Pt.^{31, 32} This effect was attributed to the substrate- induced strain.³² Generally, the finite size effects are predicted to cause significant deviations of Debye temperature from its bulk limit for very small particle sizes: for Au, the nanoparticle size should be smaller than 5nm, for its Debye temperature to start decreasing relative to the bulk.⁴⁷

Experimental data that can be used to obtain Debye temperature in NPG are scarce, and so are theoretical estimations. Fujita et al,⁴⁹ report very similar phonon scattering in NPG to bulk gold, indicating a similarity in phonon density of states and

thus similar Debye temperatures for NPG and bulk gold. Our result for $\Theta_D = 174$ K in NPG (Table 1) is in agreement with that work. On the other hand, this high value Θ_D is in contrast with theoretical predictions of Xia et al,¹³ of very low Debye temperature (23 K) in NPG. In that work, Debye temperature was estimated from the bulk elastic constants.

One important conclusion from the combination of all thermodynamic data collected in this experiment is that the metallic bonding in the NPG is anisotropic. Had it been isotropic, the ensemble-average pair distribution function would have been unimodal, and the average Au-Au pair would be characterized by an effective pair potential with the force constant k , *vide supra*. As shown in Table 1, the force constant in the NPG is smaller than in bulk Au. Hence, the Au-Au bonds in NPG should be shifted from their equilibrium positions corresponding to $\langle y \rangle = 0$ at any given temperature, namely, their lengths should increase relative to the bulk, since $k = k_0 + 6k_3\langle y \rangle$ and k_3 is negative (Eq. (2) and Table 1). In our experiment, we observe a marked decrease, not an increase, of the average bond length in the NPG relative to the bulk, i.e., the experimentally determined $\langle y \rangle$ was negative, not positive (Fig. 4), which contradicts the assumption that the bond length distribution is unimodal.

We find that our system can be better described using the model proposed by Kästle et al,⁴⁴ who proposed that the phonon spectrum of gold thin films is a superposition of the bulk and the surface spectra, weighted with the surface-to-volume fraction of Au atoms. In that work, Kästle et al, followed theoretical calculations of Al Rawi et al, to assume that three layers of Au atoms have the same low Debye temperature.⁵⁰ They further proposed that the rest of the atoms have bulklike Debye temperature, $\Theta_{D,bulk}$.⁴⁴ The surface value $\Theta_{D,surface} = 83$ K was found from LEED experiments on (111) and (110) surfaces, and 82 K was obtained for (100) surface in Au single crystals.⁵¹ We adopt a similar approach by assuming that the bond length disorder of the first nearest neighbor Au atoms is enhanced when the both atoms are near the pore surface, while the disorder is bulk-like for the rest of the bonds. Since each group of bonds must have unique Debye temperatures, we can therefore approximate the apparent

Debye temperature $\tilde{\Theta}_D$ as the weighted average of the bulk and surface Debye temperatures:

$$\tilde{\Theta}_D = \frac{N_B}{N} \Theta_{D,\text{bulk}} + \frac{N_S}{N} \Theta_{D,\text{surface}}, \quad (3)$$

where N_B and N_S are the corresponding numbers of 1NN Au-Au bonds, and N is the total number of the 1NN bonds. The numbers of each type of bonds can be expressed in terms of the total numbers of atoms within each group (bulk, n_B , or surface, n_S) and their respective coordination numbers of nearest neighbors: $Z_B = 2N_B/n_B$, $Z_S = 2N_S/n_S$, yielding:

$$\tilde{\Theta}_D = \frac{Z_B}{Z_B + Z_S \xi} \Theta_{D,\text{bulk}} + \frac{Z_S \xi}{Z_B + Z_S \xi} \Theta_{D,\text{surface}}, \quad (4)$$

where ξ is the surface-to-volume ratio of Au atoms. We assume that the surface Au atoms with lower Debye temperature are located within m monolayers from the (111)-terminated pore surface (this choice ensures that the so obtained value of m is the upper limit of the number of surface layers). The volume occupied by these surface atoms is $V_0 = mdA$, where $d = 2.35 \text{ \AA}$ is the d_{111} spacing for Au, and A is the total surface area of the NPG pores. Within this approximation ξ can be evaluated as:

$$\xi = \frac{n_S}{n_B} = \frac{V_0/V}{1 - V_0/V} = \frac{md\eta}{1 - md\eta}, \quad (5)$$

where $\eta = A/V = 9.2 \times 10^7 \text{ m}^{-1}$, as described in Section IV. Using the measured values of $\tilde{\Theta}_D = 174 \text{ K}$, $\Theta_{D,\text{bulk}} = 182 \text{ K}$ (Table I) and $\Theta_{D,\text{surface}} = 83 \text{ K}$ (Ref. ⁵¹), and assuming that $Z_B = Z_S = 12$ (as expected for face-centered cubic structure), we use Eqs. (4) and (5) to estimate m , the number of surface layers with lower Debye temperature. We obtain the upper limit of $m = 3.7 \pm 0.4$, in good agreement with Kästle et al,⁴⁴ (*vide supra*) and Al-Rawi et al,⁵⁰ who estimated theoretically that enhancement of atomic disorder near the

surface may affect atoms as deep as three layers from the surface. The experimental uncertainty in m is dominated by uncertainty in η , which has a relative error of 10%.

VI. Conclusions

In conclusion, our measurements of structural and vibrational characteristics of nanoporous gold resulted in several new effects that are markedly non-bulklike. We obtained that the Au-Au interatomic distances, the thermal expansion coefficient and the Debye temperature, are all reduced compared to the bulk gold. Reduction of the nearest neighbor distances in NPG by ca. 0.01 Å compared to the bulk is attributed to the surface tension caused, in turn, by the finite size effect of the NPG ligaments. Reduction of the Debye temperature in NPG by 5% compared to bulk gold was interpreted in the framework of the bimodal distribution of surface and bulk bonds. Using this model, and the previously measured value of surface Debye temperature, we estimate that the surface bonds with low Debye temperature extend within up to 4 layers of Au atoms located on the pore surface.

These findings indicate that the properties of nanoporous gold are affected by the dimensions of the NPG ligaments that influence both the Au-Au distance reduction, and the surface to volume ratio of Au atoms responsible for the Debye temperature reduction. Since both the pore size and the size of the ligaments, can be controlled by the NPG dealloying time,⁵² our results offer a possibility to rationally design the NPG with desired thermodynamic properties. An additional opportunity that emerges from measuring the set of pair potential characteristics in the NPG is the possibility to control the static and dynamic bond length disorder via the amount of strain in the films by varying their annealing time. Nanoscale strain is an important descriptor of catalytic activity of nanocatalysts, and our analysis method offers a direct method of its control, and evaluation. Further studies are required to confirm such capabilities, and they are presently underway.

Acknowledgments

AIF and RV acknowledge the support of this work by the U.S. DOE Grant No. DE-FG02-03ER15476. X19A and X18B beamlines are supported, in part, by

Synchrotron Catalysis Consortium (U. S. DOE Grant No. DE-FG02-05ER15688). BD and DL were supported as part of the Catalysis Center for Energy Innovation, an Energy Frontier Research Center funded by the U.S. Department of Energy, Office of Science, Office of Basic Energy Sciences under Award Number DE-SC00010004. This research was partly supported by JST-PRESTO and Sekisui research foundation.

References

- 1 A. Wittstock, V. Zielasek, J. Biener, C. M. Friend, and M. Bäumer, *Science* **327**, 319 (2010).
- 2 V. Zielasek, B. Jürgens, C. Schulz, J. Biener, M. M. Biener, A. V. Hamza, and M. Bäumer, *Angewandte Chemie International Edition* **45**, 8241 (2006).
- 3 C. Xu, J. Su, X. Xu, P. Liu, H. Zhao, F. Tian, and Y. Ding, *Journal of the American Chemical Society* **129**, 42 (2006).
- 4 S. O. Kucheyev, J. R. Hayes, J. Biener, T. Huser, C. E. Talley, and A. V. Hamza, *Applied Physics Letters* **89**, 053102 (2006).
- 5 A. Wittstock, J. Biener, and M. Bäumer, *Physical Chemistry Chemical Physics* **12**, 12919 (2010).
- 6 H. Falsig, B. Hvolbæk, I. S. Kristensen, T. Jiang, T. Bligaard, C. H. Christensen, and J. K. Nørskov, *Angewandte Chemie International Edition* **47**, 4835 (2008).
- 7 B. Hvolbæk, T. V. W. Janssens, B. S. Clausen, H. Falsig, C. H. Christensen, and J. K. Nørskov, *Nano Today* **2**, 14 (2007).
- 8 K. P. McKenna and A. L. Shluger, *Journal of Physical Chemistry C* **111**, 18848 (2007).
- 9 A. Schlapka, M. Lischka, A. Groß, U. Käsberger, and P. Jakob, *Physical Review Letters* **91**, 016101 (2003).
- 10 P. Strasser, et al., *Nature Chemistry* **2**, 454 (2010).
- 11 B. Hammer and J. K. Nørskov, *Nature* **376**, 238 (1995).
- 12 K. P. McKenna, P. V. Sushko, and A. L. Shluger, *Journal of Chemical Physics* **126**, 154704 (2007).
- 13 R. Xia, J. L. Wang, R. Wang, X. Li, X. Zhang, X.-Q. Feng, and Y. Ding, *Nanotechnology* **21**, 085703 (2010).
- 14 A. Sanson, *Journal of Physics: Condensed Matter* **23**, 315401 (2011).
- 15 G. Dalba, P. Fornasini, R. Grisenti, and J. Purans, *Physical Review Letters* **82**, 4240 (1999).
- 16 O. Kamishima, T. Ishii, H. Maeda, and S. Kashino, *Solid State Communications* **103**, 141 (1997).
- 17 L. L. Araujo, P. Kluth, G. d. M. Azevedo, and M. C. Ridgway, *AIP Conference Proceedings* **882**, 392 (2007).
- 18 M. A. Marcus, L. E. Brus, C. Murray, M. G. Bawendi, A. Prasad, and A. P. Alivisatos, *Nanostructured Materials* **1**, 323 (1992).
- 19 E. A. Stern, P. Līvņš, and Z. Zhang, *Physical Review B* **43**, 8850 (1991).
- 20 G. Bunker, *Nuclear Instruments & Methods in Physics Research* **207**, 437 (1983).

21 J. Erlebacher, M. J. Aziz, A. Karma, N. Dimitrov, and K. Sieradzki, *Nature* **410**,
450 (2001).

22 Y. Ding and J. Erlebacher, *Journal of the American Chemical Society* **125**, 7772
(2003).

23 T. Fujita and M. W. Chen, *Japanese Journal of Applied Physics* **47**, 1161 (2008).

24 A. I. Frenkel, C. W. Hills, and R. G. Nuzzo, *Journal of Physical Chemistry B* **105**,
12689 (2001).

25 S. I. Zabinsky, J. J. Rehr, A. Ankudinov, R. C. Albers, and M. J. Eller, *Physical
Review B* **52**, 2995 (1995).

26 G. Bunker, *Nuclear Instruments and Methods* **207**, 437 (1983).

27 A. I. Frenkel and J. J. Rehr, *Physical Review B* **48**, 585 (1993).

28 P. Fornasini, S. Beccara, G. Dalba, R. Grisenti, A. Sanson, M. Vaccari, and F.
Rocca, *Physical Review B* **70**, 174301 (2004).

29 K. D. Machado, *Journal of Chemical Physics* **134**, 064503 (2011).

30 A. I. Frenkel, C. W. Hills, and R. G. Nuzzo, *J. Phys. Chem. B* **105**, 12689 (2001).

31 S. I. Sanchez, L. D. Menard, A. Bram, J. H. Kang, M. W. Small, R. G. Nuzzo, and
A. I. Frenkel, *Journal of the American Chemical Society* **131**, 7040 (2009).

32 B. R. Cuenya, A. I. Frenkel, S. Mostafa, F. Behafarid, J. R. Croy, L. K. Ono, and
Q. Wang, *Physical Review B* **82** (2010).

33 D. J. Sprouster, R. Giulian, L. L. Araujo, P. Kluth, B. Johannessen, N. Kirby, and
M. C. Ridgway, *Journal of Applied Physics* **109**, 113517 (2011).

34 M. Newville, *J. Synchrotron Rad.* **8**, 322 (2001).

35 P. P. Lottici, *Physical Review B* **35**, 1236 (1987).

36 A. I. Frenkel, *Journal of Synchrotron Radiation* **6**, 293 (1999).

37 A. Frenkel, *Zeitschrift Fur Kristallographie* **222**, 605 (2007).

38 A. I. Frenkel, A. Yevick, C. Cooper, and R. Vasic, *Annual Review of Analytical
Chemistry* **4**, 23 (2011).

39 G. D. Barrera, J. A. O. Bruno, T. H. K. Barron, and N. L. Allan, *Journal of
Physics: Condensed Matter* **17**, R217 (2005).

40 A. I. Frenkel, V. S. Machavariani, A. Rubshtein, Y. Rosenberg, A. Voronel, and E.
A. Stern, *Physical Review B* **62**, 9364 (2000).

41 P. Kluth, B. Johannessen, V. Giraud, A. Cheung, C. J. Glover, G. d. M. Azevedo,
G. J. Foran, and M. C. Ridgway, *Applied Physics Letters* **85**, 3561 (2004).

42 C. W. Mays, J. S. Vermaak, and D. Kuhlmann-Wilsdorf, *Surface Science* **12**, 134
(1968).

43 N. W. Ashcroft and N. D. Mermin, *Solid State Physics* (Holt, Rinehart, Winston,
1976).

44 G. Kästle, H. G. Boyen, A. Schröder, A. Plettl, and P. Ziemann, *Physical Review
B* **70**, 165414 (2004).

45 W. B. Pearson, *Handbook of Lattice Spacings and Structure of Metals and Alloys*
(Pergamon, Oxford, 1958).

46 M. Dubiel, S. Brunsch, and L. Troger, *J. Synchrotron Rad.* **8**, 539 (2001).

47 S. Xiong, W. Qi, Y. Cheng, B. Huang, M. Wang, and Y. Li, *Physical Chemistry
Chemical Physics* **13** (2011).

48 T. Comaschi, A. Balerna, and S. Mobilio, *Physical Review B* **77**, 075432 (2008).

- 49 T. Fujita, H. Okada, K. Koyama, K. Watanabe, S. Maekawa, and M. W. Chen,
Physical Review Letters **101**, 166601 (2008).
- 50 A. N. Al-Rawi, A. Kara, and T. S. Rahman, Physical Review B **66**, 165439
(2002).
- 51 M. Kostelitz and J. L. Domange, Solid State Communications **13**, 241 (1973).
- 52 L. H. Qian and M. W. Chen, Applied Physics Letters **91**, 083105 (2007).

Table 1. Numerical results for the Einstein and Debye temperatures, linear thermal expansion coefficient and pair potential parameters obtained by EXAFS analysis in bulk Au, Ag and NPG.

	Θ_E (K)	Θ_D (K)	$\alpha(K^{-1}) (\times 10^5)$	k (N/m)	$k_3(N/m^2) (\times 10^{-11})$
Au bulk	143(1)	182(2)	1.4(1)	58.5(2)	-3.3(3)
Ag bulk	178(2)	226(3)	1.5(2)	49.3(2)	-2.5(3)
NPG	137(2)	174(2)	1.0(4)	53.1(1)	-1.9(7)

Figure Captions

Figure 1. SEM micrograph of NPG foil with characteristic ligament length scale of ca. 21 nm.

Figure 2. a) k^2 -weighted (inset) and Fourier transform magnitudes EXAFS data for the Au bulk and the NPG samples measured at 298 K. The k -range in Fourier transforms was from 2 to 18 \AA^{-1} . b) Fourier transform magnitudes of the k^2 -weighted EXAFS data of the NPG measured at different temperatures. The k -range in Fourier transforms was from 2 to 12 \AA^{-1} .

Figure 3. Fourier transform magnitudes of the k^2 -weighted data (black) and fit (red) of the NPG samples measured at the 163 K and 393 K (inset) temperatures. The k -ranges for Fourier transforms were from 2.4 to 18.5 \AA^{-1} and from 2.4 to 15.0 \AA^{-1} , respectively. The fitting ranges were from 2.0 to 3.4 \AA and from 1.7 to 3.4 \AA , respectively.

Figure 4. Au-Au distances in the bulk Au and NPG. Connecting lines are guides to the eye. Vertical line indicates the temperature (500 K) at which NPG coarsens.

Figure 5. a) Mean square Au-Au bond length disorders in the bulk Au and NPG. Best fits with Eq. (1) to each series are shown as dashed lines. The increase in slope in the NPG data relative to the bulk indicates the decreased force constant (and thus decreased Einstein and Debye temperatures) in the NPG compared to the bulk. b) The third cumulants of the Au-Au bond in the bulk Au and NPG shown as a function of T^2 . Best fits with Eq. (2) are shown as dashed lines. Vertical lines correspond to the temperature (500 K) at which NPG coarsens.

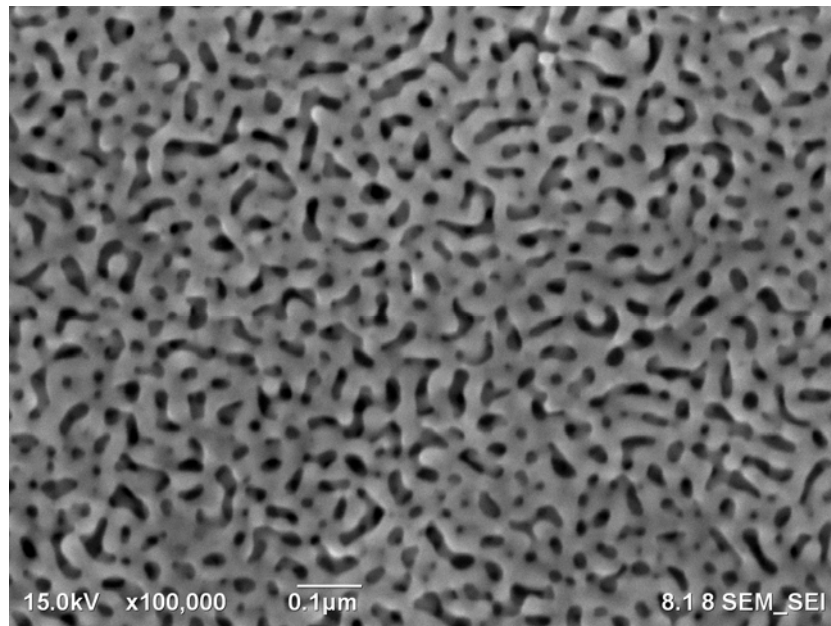


Figure 1. Frenkel *et al.*

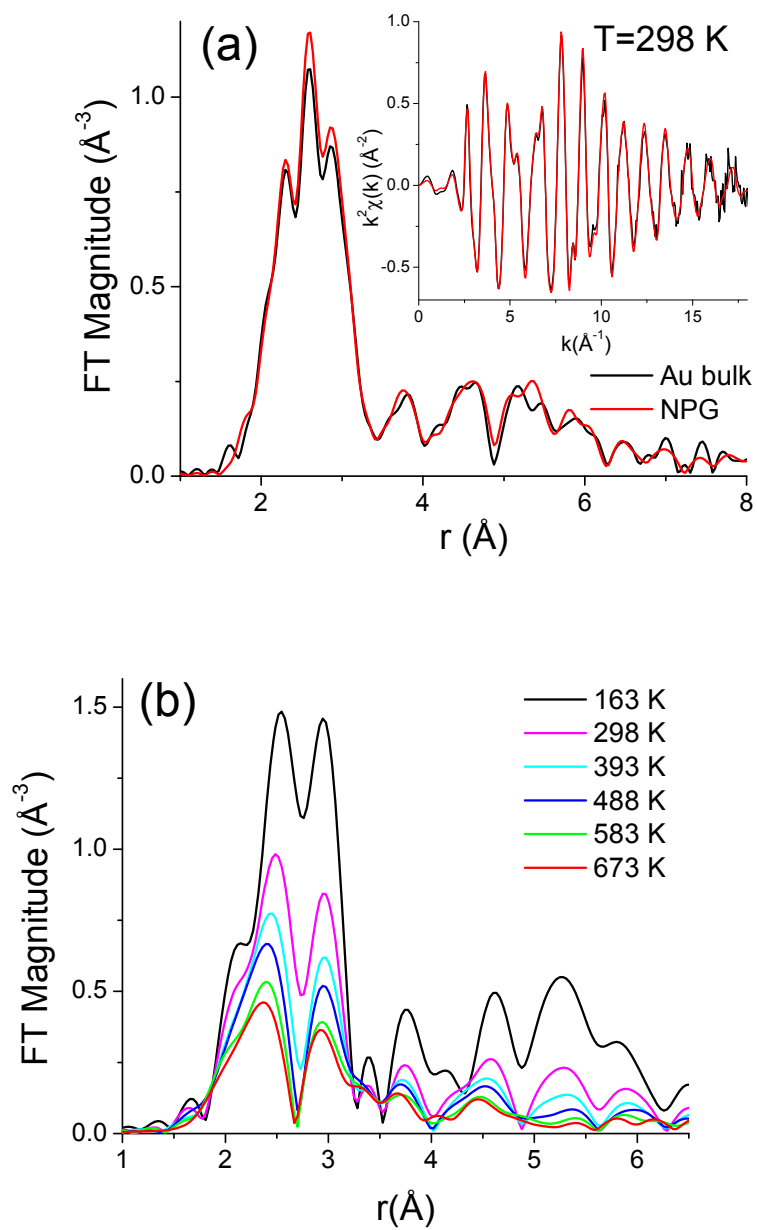


Figure 2. Frenkel *et al.*

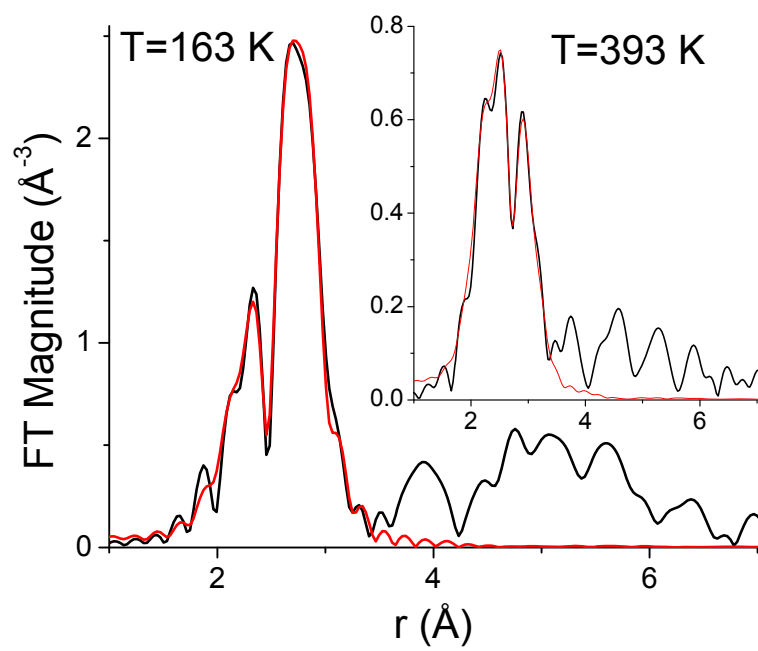


Figure 3. Frenkel *et al.*

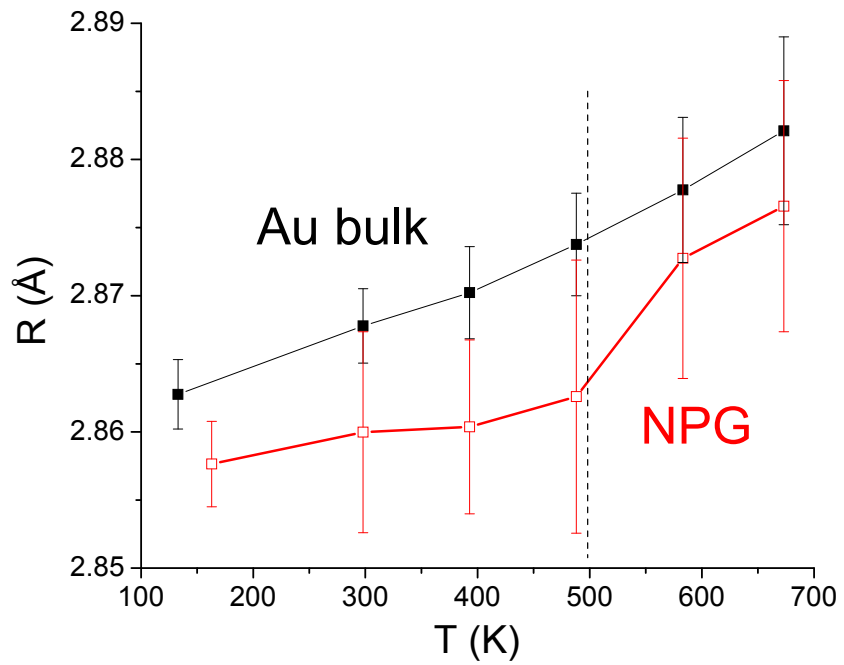


Figure 4. Frenkel *et al.*

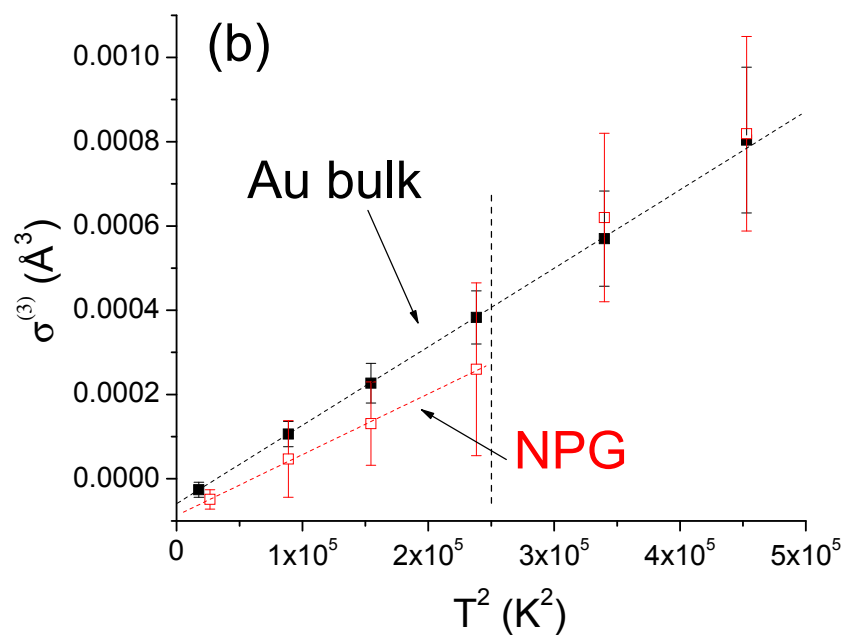
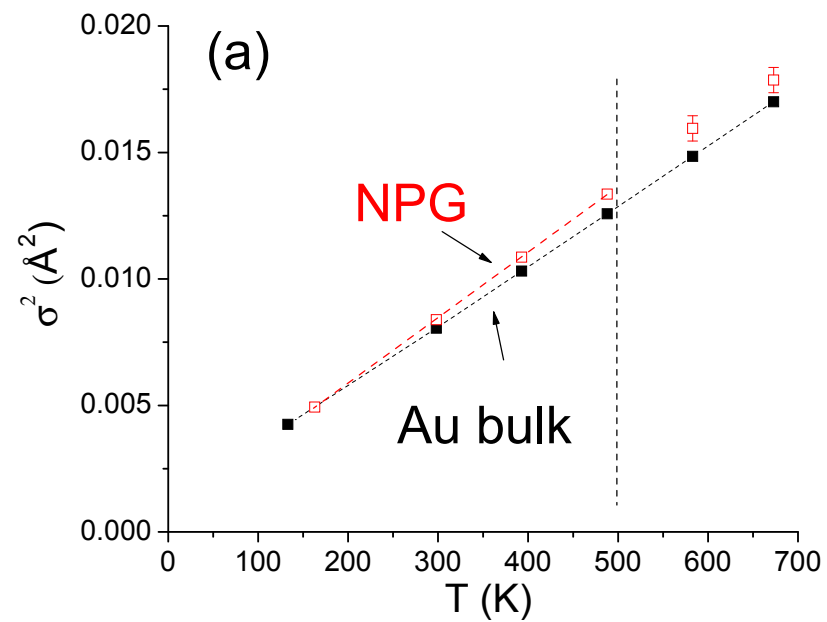


Figure 5. Frenkel *et al.*